LKB1 Inactivation Dictates Therapeutic Response of Non-Small Cell Lung Cancer to the Metabolism Drug Phenformin

David B. Shackelford,[1,4,5,*] Evan Abt,[4,5] Laurie Gerken,[1] Debbie S. Vasquez,[1] Atsuko Seki,[3] Mathias Leblanc,[1] Liu Wei,[4] Michael C. Fishbein,[3] Johannes Czernin,[4] Paul S. Mischel,[3,4,6] and Reuben J. Shaw[1,2,*]

[1]Molecular and Cell Biology Laboratory
[2]Howard Hughes Medical Institute
Dulbecco Center for Cancer Research, The Salk Institute for Biological Studies, La Jolla, CA 92037, USA
[3]Department of Pathology and Laboratory Medicine
[4]Molecular and Medical Pharmacology
[5]Pulmonary and Critical Care Medicine
David Geffen UCLA School of Medicine, Los Angeles, CA 90095, USA
[6]Present address: Laboratory of Molecular Pathology, Ludwig Institute for Cancer Research, University of California at San Diego, La Jolla, CA 92093, USA
*Correspondence: dshackelford@mednet.ucla.edu (D.B.S.), shaw@salk.edu (R.J.S.)
http://dx.doi.org/10.1016/j.ccr.2012.12.008

SUMMARY

The LKB1 (also called STK11) tumor suppressor is mutationally inactivated in ∼20% of non-small cell lung cancers (NSCLC). LKB1 is the major upstream kinase activating the energy-sensing kinase AMPK, making LKB1-deficient cells unable to appropriately sense metabolic stress. We tested the therapeutic potential of metabolic drugs in NSCLC and identified phenformin, a mitochondrial inhibitor and analog of the diabetes therapeutic metformin, as selectively inducing apoptosis in *LKB1*-deficient NSCLC cells. Therapeutic trials in Kras-dependent mouse models of NSCLC revealed that tumors with *Kras* and *Lkb1* mutations, but not those with *Kras* and *p53* mutations, showed selective response to phenformin as a single agent, resulting in prolonged survival. This study suggests phenformin as a cancer metabolism-based therapeutic to selectively target LKB1-deficient tumors.
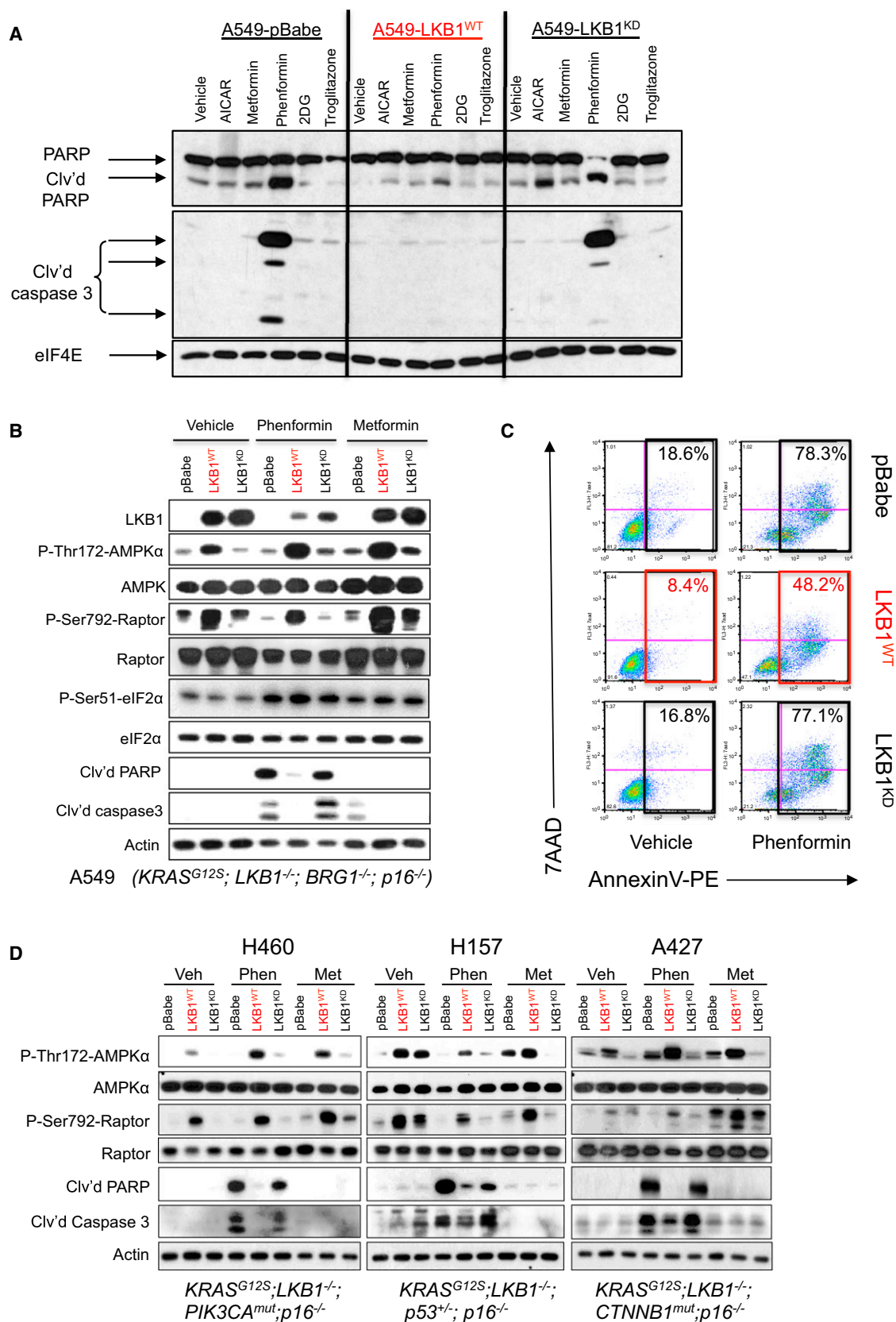
INTRODUCTION

The gene encoding the serine/threonine kinase LKB1 was identified originally as the tumor suppressor gene responsible for the inherited cancer disorder Peutz-Jeghers syndrome (Hemminki et al., 1998). *LKB1* is also the second most commonly mutated tumor suppressor in sporadic human lung cancer (after *TP53*), particularly in multiple subtypes of NSCLC (Sanchez-Cespedes et al., 2002). *LKB1* is mutated in at least 15%–30% of NSCLCs, but the true frequency might be even higher because of difficulties in detecting inactivating lesions (Ding et al., 2008; Gill et al., 2011; Ji et al., 2007). Roughly half of the NSCLC tumors with *LKB1* mutation also bear activating *KRAS* mutations, and current estimates suggest that 7%–10% of all NSCLC are comutated for *KRAS* and *LKB1* (Ding et al., 2008; The Cancer Genome Atlas). Studies in genetically engineered mouse models have shown that simultaneous activation of *Kras*[G12D] and biallelic deletion of *Lkb1* in the lung dramatically increases tumor burden and metastasis (Carretero et al., 2010; Chen et al., 2012; Ji et al., 2007).

Biochemical and genetic analyses in worms, flies, and mice have shown that LKB1 is the major kinase phosphorylating the AMP-activated protein kinase (AMPK) under conditions of energy stress across metazoans (Hardie et al., 2012). AMPK is a highly conserved energy sensor and modulator of cell growth and metabolism that is activated under conditions of low intracellular ATP. Activated AMPK regulates cell growth at least in

Significance

Targeted therapeutics are making significant advances in subsets of NSCLC bearing activated oncogenic targets, such as *EGFR* and *ALK*. More prevalent in NSCLC are mutations in the *KRAS* oncogene coincident with mutations in the *LKB1* or *p53* tumor suppressor genes. Currently, there are limited options for *LKB1* mutant tumors. Here, we define the hypersensitivity of *LKB1*-defective cells to metabolic stress and test the therapeutic use of phenformin, a mitochondrial inhibitor and a former type 2 diabetes drug, in mouse models of NSCLC. Phenformin as a single agent reduced tumor burden and prolonged survival in *Kras;Lkb1* compound mutant mice but not *Kras;p53* mice. These findings suggest phenformin or related agents may find clinical utility to treat NSCLC bearing *LKB1* mutations.

A

B

A549   (KRAS^{G12S}; LKB1^{-/-}; BRG1^{-/-}; p16^{-/-})

C

D

H460

H157

A427

KRAS^{G12S};LKB1^{-/-};
PIK3CA^{mut};p16^{-/-}

KRAS^{G12S};LKB1^{-/-};
p53^{+/-}; p16^{-/-}

KRAS^{G12S};LKB1^{-/-};
CTNNB1^{mut};p16^{-/-}

(legend continued on next page)

part through inhibition of mTORC1 signaling achieved through dual phosphorylation of TSC2 (Inoki et al., 2003) and Raptor (Gwinn et al., 2008). AMPK is also hypothesized to maintain energy homeostasis in part by targeting defective mitochondria for autophagy (Egan et al., 2011) and control of fatty acid metabolism (Jeon et al., 2012).

The diabetes therapeutic biguanide compounds metformin and phenformin have been shown to inhibit complex I of the mitochondria (Dykens et al., 2008; El-Mir et al., 2000; Owen et al., 2000), resulting in increases in intracellular AMP and ADP that bind to the gamma regulatory subunit of AMPK and trigger LKB1-dependent phosphorylation of AMPK (Hawley et al., 2010). Consistent with activation of a low energy checkpoint, metformin treatment has been found to reduce tumor growth in xenograft, transgenic, and carcinogen-induced mouse cancer models (Algire et al., 2011; Anisimov et al., 2005; Buzzai et al., 2007; Memmott et al., 2010). Epidemiological studies revealed that diabetic patients taking metformin show a statistically significant reduced tumor incidence (Dowling et al., 2012; Evans et al., 2005). Given the extensive knowledge on the safety and use of metformin, there is increasing interest in using metformin as an anticancer agent (Taubes, 2012). Phenformin is a 50-fold more potent inhibitor of mitochondrial complex I than metformin (Dykens et al., 2008; Owen et al., 2000). Moreover, uptake of metformin, but not phenformin, into tissue appears to require the expression of Organic Cation Transporter 1 (OCT1), which is highly expressed in hepatocytes but not elsewhere (Shu et al., 2007). Consistent with greater potency and broader tissue bioavailability, phenformin delayed tumor progression in a $Pten^{+/-}$ spontaneous lymphoma mouse model to a much greater extent than metformin (Huang et al., 2008).

In most settings metabolic stress induces a cytostatic growth arrest, dependent in part on AMPK. However, in cells lacking a functional LKB1 pathway, metabolic stress has been demonstrated to result in rapid apoptosis as the cells are unable to sense the energy stress and activate mechanisms to restore energy homeostasis (Shaw et al., 2004). Similar effects are seen in autophagy-defective cells that are unable to restore metabolism under low nutrient conditions (Jin et al., 2007). Here, we directly examine the hypothesis that LKB1-deficient lung tumors may be targeted with metabolic drugs.

RESULTS

Phenformin Selectively Induces Apoptosis in LKB1-Deficient NSCLC Cell Lines

We previously reported that nontransformed murine embryonic fibroblasts and HeLa cervical carcinoma cells deficient of LKB1 exhibit increased apoptosis in response to metabolic stresses, including glucose deprivation and the AMP mimetic AICAR (Shaw et al., 2004). However, whether tumor cells undergo growth arrest or apoptosis following a particular cellular insult is dependent in part on the full constellation of oncogenic mutations present in the cell. We sought to determine whether NSCLC cell lines bearing KRAS mutations and lacking LKB1 would show enhanced rates of apoptosis following metabolic stress treatments compared to isogenic lines in which wild-type LKB1 had been restored.

We performed our initial studies using the *KRAS* mutant and *LKB1*-deficient NSCLC cell line A549 and derivatives with retrovirally introduced stable expression of wild-type LKB1 cDNA (LKB1^{WT}), a kinase-inactive LKB1 cDNA (LKB1^{KD}), or an empty vector (pBABE). These cells were treated with a variety of drugs with established roles in causing metabolic stress: metformin, phenformin, the cell permeable AMP-mimetic AICAR, the glycolysis inhibitor 2-deoxyglucose, or the thiazolidinedione compound troglitazone that acts as a mitochondrial inhibitor in addition to effects on PPARγ (Hardie et al., 2012). Immunoblotting for cleaved caspase 3 and cleaved PARP as markers of apoptosis induction, we observed that, of the agents tested, only phenformin induced apoptosis in the cells lacking functional LKB1 (Figure 1A). Although both biguanides lowered ATP production in A549 cells (Figure S1A available online), phenformin reduced cellular ATP more, consistent with previous studies (Owen et al., 2000; Dykens et al., 2008). The ATP-lowering effect of both drugs was modestly blunted when wild-type LKB1 was present, consistent with the current model that AMPK acts to restore ATP levels and with previous findings in wild-type and *Lkb1*-deficient myocytes (Sakamoto et al., 2005). Consistent with a greater impact on ATP levels, phenformin but not metformin induced apoptosis in A549 cells lacking functional LKB1 by multiple measures: cleaved PARP and caspase 3 immunoblot (Figure 1B), activated caspase 3/7 luminescence assay (Figure S1B), and flow cytometry measuring AnnexinV and 7AAD staining (Figure 1C).

As human daily doses of metformin routinely run between 500 and 1,000 mg, and phenformin was given in the range of 50 to 100 mg previously when used clinically, we performed a direct comparison of metformin to phenformin at ratios of 1:1 and 10:1 in time course experiments in isogenic A549 cell lines. At early time points (8 or 12 hr) metformin at 2 or 20 mM or phenformin at 2 mM similarly induced AMPK signaling as shown by increased P-AMPK and P-Raptor levels (Figure S1C). However, only phenformin induced higher levels of cellular stress, triggering induction of P-Ser51 eIF2α and its downstream target CHOP, and markers of apoptosis at later times (Figures 1B and

Figure 1. Phenformin Selectively Induces Apoptosis in *LKB1*$^{-/-}$ NSCLC Tumor Cells

(A) A549 human NSCLC cells expressing the pBabe vector (A549-pBabe), full-length LKB1 (A549-LKB1^{WT}), or kinase-dead LKB1 (A549-LKB1^{KD}) were treated with vehicle (DMEM), AICAR (2 mM), metformin (20 mM), phenformin (2 mM), 2DG (10 mM), or troglitazone (25 μM) for 48 hr. Lysates were immunoblotted with the indicated antibodies.

(B) A549 isogenic cell lines were treated for 24 hr with vehicle (DMEM), 2 mM phenformin, or 20 mM metformin. Lysates were immunoblotted with the indicated antibodies.

(C) Fluorescence-activated cell sorting (FACS) on cells stained with AnnexinV-PE and 7AAD following 48 hr treatment with vehicle or 2 mM phenformin.

(D) H460, H157, or A427 cell lines expressing the pBabe vector (pBabe), full-length WT LKB1 (LKB1^{WT}), or kinase-dead LKB1 (LKB1^{KD}) were treated for 24 hr with vehicle (DMEM), 2 mM phenformin, or 20 mM metformin. Lysates were immunoblotted with the indicated antibodies. Cancer gene driver mutations found in these cell lines listed under each.

See also Figure S1.

S1C). eIF2α phosphorylation and upregulation of CHOP is observed in response to a diverse set of cellular stresses, including the unfolded protein response, nutrient deprivation, and mitochondrial stress (Muaddi et al., 2010; Ye et al., 2010; Chae et al., 2012). This suggests that although AMPK activation is a rapid and sensitive sensor of ATP loss, its signal plateaus and does not continue to increase with greater ATP loss, when additional stress sensing pathways like eIF2α kinases may be engaged. Note that LKB1 did not impact P-eIF2α or CHOP levels (Figures 1B and S1C), indicating that eIF2α signaling is behaving here as an AMPK-independent pathway.

To examine how widely the sensitivity of cell lines to apoptosis by phenformin treatment is dictated by LKB1, we tested a panel of NSCLC lines that all had KRAS and LKB1 mutations, but each contained additional unique mutations. Isogenic derivatives of each cell line expressing wild-type or kinase-dead LKB1 were established and examined for sensitivity to phenformin or metformin. Despite each cell line containing different additional mutations, their sensitivity to undergo apoptosis following phenformin treatment was dictated by the *LKB1* genotype in all cases (Figures 1D and S1B). Protection from phenformin-induced apoptosis was also observed with *LKB1*-reconstituted NSCLC and cervical cell lines H838 and HeLa, respectively, that are deficient for *LKB1* but wild-type for *KRAS* (Figure S1B). Taken altogether, these data indicate that LKB1 dictates the sensitivity of a variety of cancer cell lines to phenformin-induced metabolic catastrophe regardless of the other tumor mutations present.

Developing Genetically Engineered Mouse Models of NSCLC that Can Be Monitored by Bioluminescence Longitudinally

Though a handful of studies have begun examining metabolic drugs in xenograft models, of particular concern is that subcutaneous placing a mass of tumor cells into an nonvascularized environment and without appropriate basement membrane attachment will itself result in severe metabolic stress and AMPK activation (Jeon et al., 2012; Laderoute et al., 2006), thus altering the very pathways being tested here for their impact on therapeutic outcome. To better model LKB1-deficient tumors, we took advantage of the well-characterized adenoviral cre-induced NSCLC models initiated by a conditionally activated *K-ras* oncogene (Lox-Stop-Lox-*Kras*^G12D, hereafter called *Kras*), combined with mice bearing floxed alleles of *p53* or *Lkb1* (Farago et al., 2012). As previously reported (Chen et al., 2012; Ji et al., 2007), when *p53* deficiency or *Lkb1* deficiency is combined with Kras activation, there is a dramatic increase in tumor burden leading to metastasis and earlier death,10–12 weeks post-cre administration in both *Kras;Lkb1*^L/L and *Kras;p53*^L/L mice compared to 25+ weeks in *Kras* mice. To facilitate noninvasive imaging of tumor burden in longitudinal studies on these mice following therapeutic intervention, we crossed *Kras*, *Kras;Lkb1*^L/L, or *Kras;p53*^L/L mice with a ROSA26 lox-stop-lox *luciferase* allele (hereafter called *Luc*) (Safran et al., 2003) to generate *Kras;Luc* (K_{luc}), *Kras;Lkb1*^L/L;*Luc* (KL_{luc}), or *Kras;p53*^L/L;*Luc* (KP_{luc}) mice. We bred these genotypes into the FVB background whose white coat allowed for noninvasive bioluminescent luciferase imaging without fur removal (Figures S2A–S2C). On the FVB genetic background, KL_{luc} and KP_{luc} mice exhibited comparable extents of tumor burden and similar latency.

We demonstrated that the bioluminesence output from the ROSA26-encoded luciferase was proportional to tumor burden (see the Supplemental Experimental Procedures). Analyzing lung tumor progression in K_{luc}, KL_{luc}, and KP_{luc} mice, we detected bioluminescence as early as 4 weeks in KL_{luc} and KP_{luc} mice and confirmed the presence of adenomas by hematoxylin and eosin (H&E) staining (Figures 2A–2D; Figures S2A–S2C). At 6 weeks, tumors in the KL_{luc} and KP_{luc} mice began to change from adenomatous features to a more malignant tumor phenotype typical of carcinomas (Figure 2D). The most common histologic pattern in both KL_{luc} and KP_{luc} mice were high-grade invasive papillary adenocarcinoma. Squamous cell and adenosquamous carcinoma were commonly observed tumor subtypes in KL_{luc} mice, as previously noted (Ji et al., 2007). Interestingly, KL_{luc} mice also displayed severe mucinous bronchiolar-epithelial adenocarcinoma (mBEAC) and bronchial mucinous papillary lesions, which were rarely seen in K_{luc} or KP_{luc} mice (Figure S2D). Of note, *LKB1* is frequently mutated in NSCLC patients with mucinous bronchiolar adenocarcinoma (Osoegawa et al., 2011).

Next, we characterized AMPK and mTORC1 signaling in K_{luc}, KL_{luc}, and KP_{luc} lung tumors by immunohistochemical staining for P-AMPK and P-4E-BP1 (Figure 2E). Notably, the KL_{luc} tumors contained the highest degree of P-4E-BP1, consistent with mTORC1 being particularly hyperactive in LKB1-deficient tumors. *Lkb1* deletion in the *Kras* mutant tumors was also accompanied by near-complete loss of P-AMPK as seen in many other tissues previously (Figure 2E).

Phenformin Activates the AMPK Signaling Pathway in K_{luc} and KP_{luc} Lung Nodules

To further examine their prospects as anticancer agents, we compared the bioavailability of metformin and phenformin in mouse lung tissue. Phenformin is a more lipophilic molecule compared to metformin (Figure S3A) and, unlike metformin requiring OCT1 for cell entry (Shu et al., 2007), readily permeates cells and tissues (Hawley et al., 2010; Huang et al., 2008). We performed intraperitoneal (i.p.) injections of vehicle, metformin, or phenformin on wild-type mice and isolated lung tissue at 1, 4, and 8 hr postinjection. Immunoblot analysis showed a weaker activation of the AMPK signaling pathway by metformin that only was observed at the 1 hr time point, unlike phenformin, which showed a robust activation at 4 hr postinjection (Figure 3A). However, mice bearing lung tumors did not tolerate daily i.p. injections over multiple weeks, and therefore phenformin was administered through the drinking water of mice fed ad libitum, as previously described (Appleyard et al., 2012; Huang et al., 2008). Quantitative analysis of P-AMPK staining in KP_{luc} lung tumors from mice treated for 2 weeks showed greater activation of AMPK with phenformin than metformin (Figures S3B and S3C). As expected, no induction of P-AMPK was ever seen in KL_{luc} tumors. Measurement of metformin and phenformin in blood plasma of mice by mass spectrometry revealed that levels of both were steady over days when administered via drinking water (Figure S3D).

Immunoblot analysis of snap-frozen K_{luc}, KL_{luc}, and KP_{luc} lung tumor nodules revealed that tumors from K_{luc} and KP_{luc} mice treated with phenformin had higher levels of AMPK activation compared to vehicle treated mice, whereas KL_{luc} lung tumors showed a lack of AMPK signaling as expected (Figure 3B).
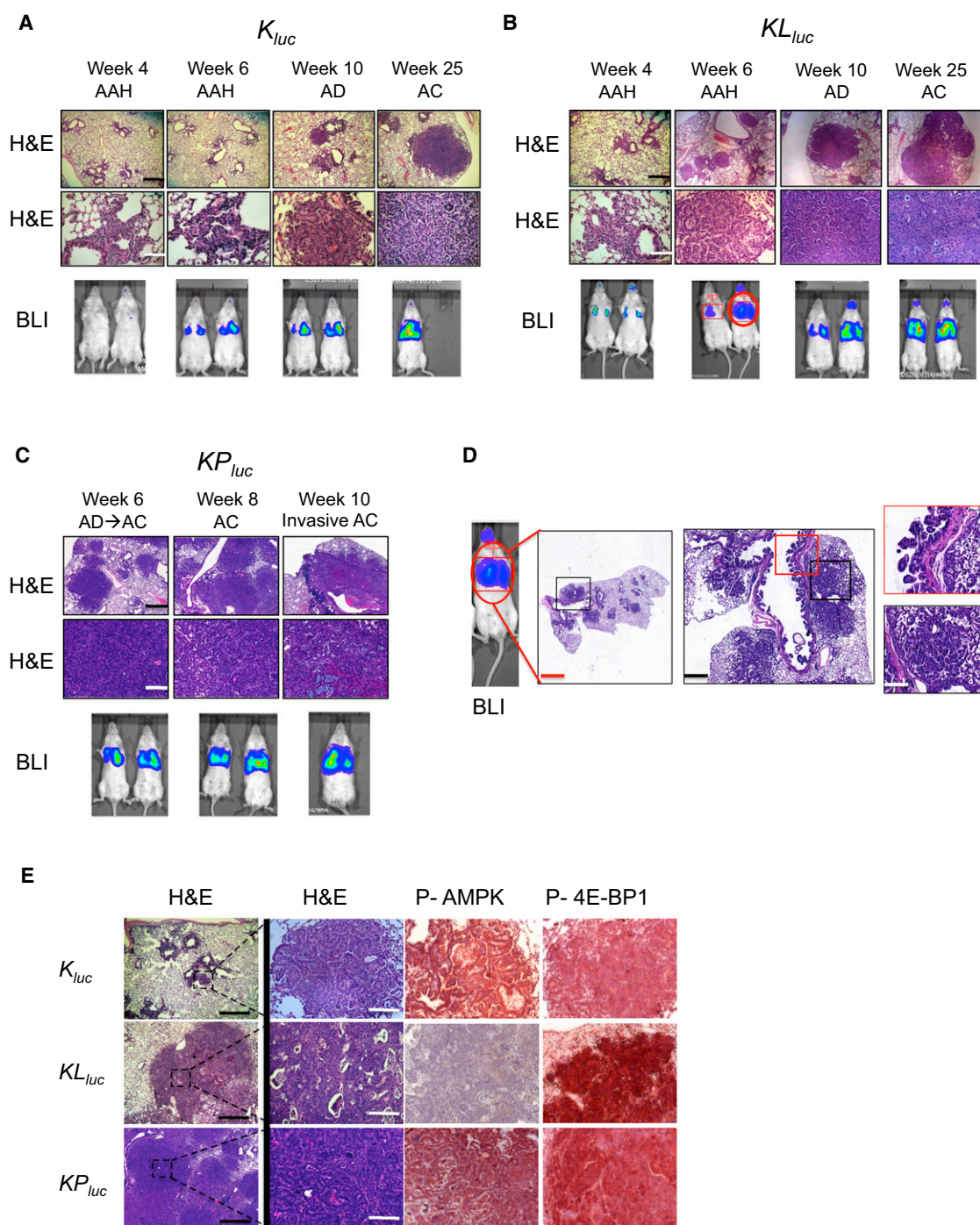
Figure 2. Time Course of Tumor Progression in K_{luc}, KL_{luc}, and KP_{luc} Lung Tumor Models

(A–C) Tumor progression in K_{luc} (A), KL_{luc} (B), and KP_{luc} (C) murine lung tumor measured by H&E staining or bioluminescence (bottom panel) at the indicated time points. Scale bars (black) = 300 μm. Scale bars (white) = 100 μm. Mice shown are representative of 10–12 mice per genotype.

(D) Detailed analysis of H&E-stained lung tumors from a KL_{luc} mouse (red circled mouse from the bottom of B) at 6 weeks post-AdCre administration. Scale bars (red) = 1 mm, (black) = 500 μm, and (white) = 100 μm.

(E) Immunohistochemical analysis of representative lung tumors from K_{luc}, KL_{luc}, and KP_{luc} mice 10 weeks post-AdCre administration. Sections were stained with H&E or the indicated antibodies. Scale bars (black) = 500 μm. Scale bars (white) = 100 μm.
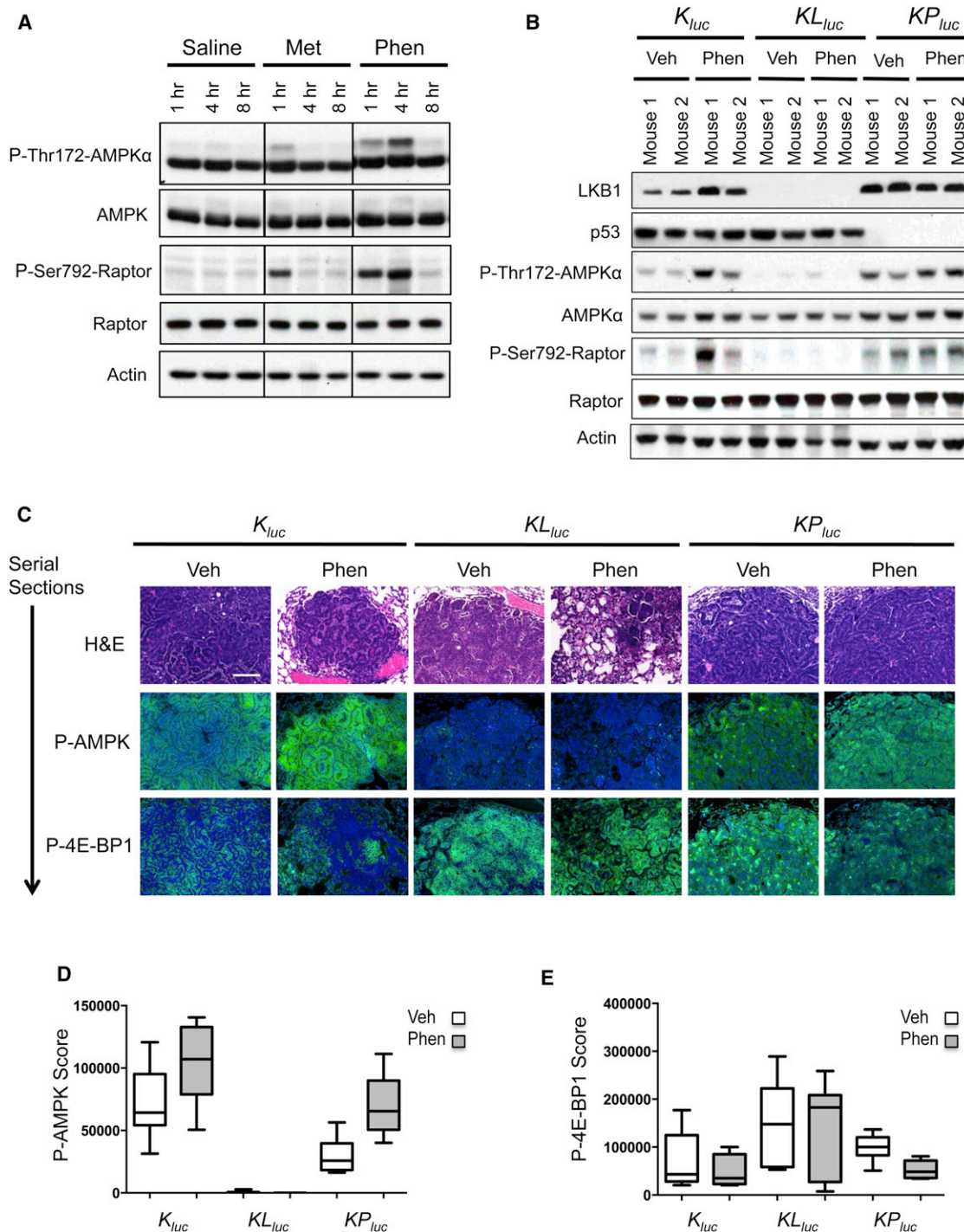
See also Figure S2.

Figure 3. Phenformin Treatment Activates AMPK Pathway in K-Ras-Driven Lung Tumors In Vivo

(A) Lung tissue lysates from wild-type FVB mice following i.p. injection of saline (0.9%), metformin (300 mg/kg), or phenformin (150 mg/kg) and immunoblotted with the indicated antibodies.

(B) Lysates of lung tumor nodules from K_{luc}, KL_{luc}, and KP_{luc} mice treated with vehicle (water) or phenformin via 5 days ad lib feeding were immunoblotted with the indicated antibodies.

(C) Representative images of K_{luc}, KL_{luc}, and KP_{luc} lung tumor sections stained with hematoxylin and eosin (H&E), P-AMPK, or P-4E-BP1. P-AMPK or P-4E-BP1 positively stained cells (in green) and nuclei (in blue). Scale bar = 100 μm.

(D and E) Box plots representing the mean P-AMPK (D) or P-4E-BP1 (E) signal from K_{luc}, KL_{luc}, and KP_{luc} lung tumors treated with vehicle or phenformin. n = 6 mice analyzed per treatment group in each genotype (K_{luc}, KL_{luc}, and KP_{luc}) treatment group.

All data are represented as the mean ± SEM.

See also Figure S3.

Normal lung lysates from wild-type FVB mice given phenformin ad libitum for 2 weeks showed an increase in AMPK signaling and lowered mTORC1 signaling, when compared to the vehicle treated mice (Figure S3E). Phenformin also increased levels of P-eIF2α and its target BiP/Grp78 in normal lung as well as in lung tumors (Figures S3E and S3F) (the CHOP antibody afore used recognized human but not mouse CHOP). There was no observed difference in IGF-IR/IR or Akt signaling between the vehicle- or phenformin-treated mice. Analysis of the AMPK activation in lung tumors by quantitative immunohistochemistry following phenformin treatment paralleled the results observed by immunoblotting (Figures 3C and 3D), and phenformin was observed to modestly reduce the mTORC1 substrate P-4E-BP1 levels in all genotypes (Figures 3C and 3E).

Lkb1$^{-/-}$ Lung Tumors Reveal Higher Levels of Apoptosis and Reduced Tumor Burden following Phenformin Treatment

Having established that phenformin had greater bioavailability and was capable of more potently inducing energy stress in tumors than metformin, we next tested phenformin as a single-agent therapeutic in the KL_{luc}, KL_{luc}, and KP_{luc} mice. Following tumor induction, we performed bioluminescent imaging (BLI) to monitor tumor growth and sorted mice into equal groups according to their BLI value to normalize the cohorts receiving vehicle or phenformin (Figures S4A–S4C). We first tested phenformin as a chemotherapeutic by initiating treatment 6 weeks postadenoviral cre delivery for the KP_{luc} and KL_{luc} mice and 9 weeks post-adenoviral cre delivery in the K_{luc} (Figure S4D) in order to target aggressively growing tumors transitioning from benign to malignant tumors (Figures 2A–2C). After 3 weeks of treatment, BLI imaging revealed modestly reduced tumor burden in mice of all genotypes receiving phenformin, but the only statistically significant decrease was in the KL_{luc} lung tumors (Figures 4A and 4B).

To better quantify tumor burden in mice, we combined BLI with quantitative histological analysis. H&E-stained lungs were imaged with morphometric software to quantify the surface area composed of tumor as opposed to normal tissue of representative cross-sections of each lung lobe for each mouse was determined (Figures S4E and S4F). Importantly, tumor burden determined by histological analysis correlated closely with BLI. KL_{luc} mice showed significant reductions in lung tumor area (Figures 4C and 4D), while modest reductions in tumor burden were also seen in both K_{luc} and KP_{luc} mice. Normalization of the tumor burden for each tumor genotype, performed by calculating the ratio of phen:veh tumor mass, showed the largest decrease in tumor burden for the KL_{luc} mice as compared to K_{luc} and KP_{luc} mice (Figure S4G). In addition, we observed no change in rate of metastasis following phenformin treatment in any of our therapeutic trials. These results demonstrate phenformin as a single agent selectively attenuates Lkb1-deficient lung tumor growth in vivo.

We next analyzed apoptosis and tumor proliferation in the lung tumors by TUNEL and Ki67 staining, respectively. Phenformin treatment modestly reduced Ki67 index in KL_{luc} tumors but not K_{luc} and KP_{luc} tumors (Figures 4E and 4F), and TUNEL staining revealed that KL_{luc} lung tumors had the highest levels of apoptotic tumor cells following phenformin (Figures 4E and

4G). Interestingly, KL_{luc} lung tumors also had higher basal levels of apoptosis compared to KP_{luc} and K_{luc} tumors, perhaps reflecting the prosurvival role of LKB1 in restoring energy homeostasis under conditions of metabolic stress, which may spontaneously arise in the context of a tumor.

Phenformin Induced a Significant Increase in Survival and Therapeutic Response in KL_{luc} Mice following Long-Term Treatment

Given the response of late-stage KL_{luc} lung tumors to phenformin treatment, we decided to treat earlier stage lung tumors in KL_{luc} and KP_{luc} mice. To better mimic the human clinical use of biguanides, we used oral gavage (o.p.) to deliver daily the maximum tolerated dose of 100 mg/kg phenformin starting at 3 weeks posttumor induction (Figure S5A). As expected, delivery of phenformin by this method resulted in AMPK pathway activation in KP_{luc} but not KL_{luc} tumor nodules (Figures S5B and S5C). Mass spectrometry on phenformin in blood plasma following o.p. delivery demonstrated a rapid uptake of phenformin followed by a steady decrease in blood plasma over 24 hr (Figure S5D). Importantly, these FVB mice are on a chow diet and nondiabetic, and the dose of phenformin used following 6 weeks of daily administration did not significantly impact blood plasma insulin levels, glucose levels, or lead to increased blood lactate levels as compared to vehicle-treated mice (Figures S5E–S5H).

The loss of LKB1 function in tumors predicts increased glycolytic metabolism and ^{18}F-fluoro-2-deoxyglucose positron emission tomography (FDG-PET) avidity as shown in gastrointestinal polyps from $Lkb1^{+/-}$ mice (Shackelford et al., 2009) and in NSCLC in mice and humans (Chen et al., 2012). Therefore, we explored the use of FDG-PET as a surrogate endstage biomarker in combination with microCT (μCT) imaging to longitudinally monitor tumor progression and response in KL_{luc} and KP_{luc} mice following phenformin treatment. KL_{luc} and KP_{luc} mice were given baseline FDG-PET and μCT scans, which were scored by a radiologist blinded to the identities of the mice. Mice in both groups were determined to be negative for tumors by both PET and CT scans and were randomly sorted into treatment groups (Figure 5C).

When phenformin was administered by o.p. for an extended time, it significantly increased survival in KL_{luc} mice compared to KP_{luc} mice (Figures 5A and 5B). Phenformin treatment resulted in delayed tumor progression in KL_{luc} but not KP_{luc} mice as shown by μCT measurements of lung tumor volume over time for individual mice in the study (Figures 5C–5E, S5J, and S5K). At 4 and 6 weeks of treatment, average lung tumor size was significantly reduced in KL_{luc} mice (Figure 5D). There was a trend toward smaller tumors in the KP_{luc} mice but did not reach statistical significance (Figure 5E). However, at endstage, there was the presence of large, advanced solid tumors of the vehicle and phenformin groups in both KL_{luc} and KP_{luc} tumor genotypes (Figure S5I). The ^{18}FDG uptake into tumors was quantified by the standardized uptake value (SUVmax) at 4 and 6 weeks of treatment. The SUVmax for phenformin-treated KL_{luc} lung tumors was significantly reduced compared to vehicle ones (Figure 5F). No difference was seen in the SUVmax for the KP_{luc} mice at these same time points (Figure 5G). These data suggest a therapeutic response in KL_{luc} lung tumors following phenformin treatment. However, the SUVmax values in endstage tumors were
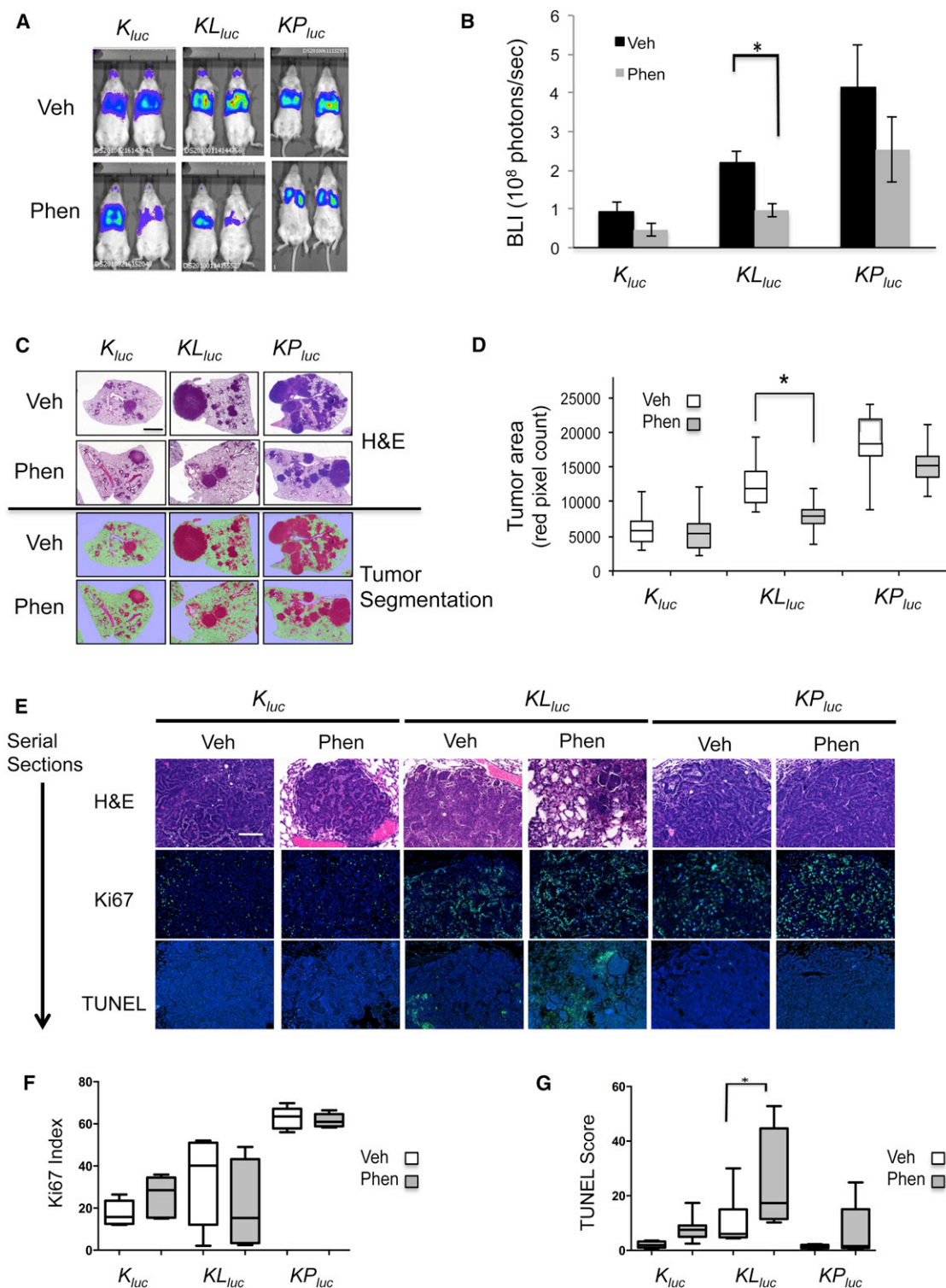
Figure 4. Phenformin Preferentially Inhibits LKB1-Deficient Lung Tumors In Vivo

(A) Representative ventral view images of bioluminescence from K_{luc}, KL_{luc}, and KP_{luc} mice. Bioluminescence imaging (BLI) performed on K_{luc} (veh, n = 11; phen, n = 12 mice), KL_{luc} (veh, n = 10; phen, n = 10 mice), and KP_{luc} (veh, n = 7; phen, n = 7 mice) following 3 weeks of treatment with vehicle (water) or phenformin via ad lib feeding.

(B) Average BLI for each treatment group of the K_{luc}, KL_{luc}, and KP_{luc} mice at 3 weeks treatment.

(C) Representative images of tumor burden in K_{luc}, KL_{luc}, and KP_{luc} mice as shown by H&E-stained lung sections (top panel) or the same images tissue segmented and pseudocolored with Inform software (bottom panel). Scale bar = 1 mm.

(legend continued on next page)

increased in both KL_{luc} and KP_{luc} mice (Figures S5L and S5M), suggesting the emergence of phenformin-resistant tumors in KL_{luc} mice (Figures S5J and S5L).

Histopathological analysis of 6 week o.p. phenformin-treated lungs revealed that KL_{luc} but not KP_{luc} lung tumors had large regions of necrosis, which was absent in the vehicle-treated controls (Figure 6A; Figure S6A). Further analysis of KL_{luc} lung sections revealed an 8-fold increase in necrotic tumor areas as shown by the presence of necrotic bodies with ghost cells (Figures 6B and 6F). Staining of KL_{luc} and KP_{luc} tumors for cleaved caspase 3 revealed a significant increase in tumor cell apoptosis in both KL_{luc} and KP_{luc} lung tumors following phenformin (Figures 6C, 6G, S6A, and S6B) but no difference in Ki67 indices in either genotype following phenformin treatment (Figures 6D, 6H, S6A, and S6C). Elevated P-AMPK levels were observed in both tumor and lung parenchyma of phenformin-treated KP_{luc} mice (Figure S6D), further reflecting that this dosing regimen was capable of inducing energy stress in these different lung cell populations. Strikingly, the abundant mucinous bronchiolar-epithelial adenocarcinoma (mBEAC), which occluded much of the upper airways in KL_{luc} mice, showed a 2-fold decrease in surface area in mice receiving phenformin compared to the vehicle group (Figures 6E and 6I). Altogether, these results indicate that phenformin as a single agent induces a tumor response in both KL_{luc} and KP_{luc} lung tumors with $Lkb1$-deficient tumors showing the most robust overall therapeutic response to phenformin.

Mitochondrial Defects May Sensitize LKB1-Deficient NSCLC Tumor Cells to Phenformin

To examine the molecular mechanism behind the selective induction of apoptosis in LKB1-deficient lung cancer cells, we analyzed signals downstream of its main target AMPK. Recently, we demonstrated that AMPK phosphorylates and activates the autophagy kinase ULK1, which is required for mitophagy and cell survival under starvation conditions (Egan et al., 2011). We previously observed an accumulation of mitochondria with defective mitochondrial membrane potential ($\Delta\psi$) in $Ampk$- and $Ulk1$-KO fibroblasts and hepatocytes (Egan et al., 2011), similar to that observed in $Lkb1$-KO hematopoetic stem cells (Nakada et al., 2010), so we examined here whether ULK1 and mitochondrial homeostasis might be disrupted in LKB1 mutant NSCLC cells. A549 cells reconstituted with functional LKB1 showed AMPK activation and its phosphorylation of endogenous ULK1 on Ser555 following phenformin treatment, paralleling phosphorylation of Raptor, another AMPK substrate (Figure 7A). Phenformin treatment also resulted in a decrease in levels of the p62/Sqstm1 protein only in the wild-type LKB1-reconstituted cells, indicative of efficient autophagy reliant on LKB1 function (Figure 7A). Importantly, p62 levels were not reduced by metformin here, perhaps reflecting the lower level of AMPK signaling from

metformin as compared to phenformin. Expression of functional LKB1 in LKB1-deficient H157 and H838 cells also restored their P-Ser555 ULK1 signal, indicating this is a general defect in LKB1-deficient NSCLC cell lines (Figure S7A). As observed previously in AMPK- and ULK1-defective fibroblasts and hepatocytes, here A549, H157, and H838 NSCLC cells defective for LKB1 function exhibited increased mitochondrial content as assayed by flow cytometry for mitotracker red staining (Figure 7B and S7B), suggesting that reconstitution of wild-type LKB1 into these LKB1-deficient NSCLC cell lines may actively induce functional mitophagy. A549-pBabe and A549-LKB1^{KD} cells had impaired $\Delta\psi$, reflecting impaired mitochondrial membrane integrity, as exhibited by the failure of JC-1 dye to accumulate in the mitochondrial membrane when compared to A549-LKB1^{WT} cells (red to green ratio of JC-1 staining in Figure 7C). Following treatment with phenformin, LKB1-deficient tumor cells showed a complete loss of mitochondrial membrane potential, whereas expression of functional LKB1 fully prevented this loss. In contrast, treatment with the mitochondrial uncoupler CCCP induced loss of $\Delta\psi$ in all cell lines, though LKB1-reconstituted cells still retained the most mitochondrial membrane potential (Figure 7C). As one measure of functionality of the mitochondria in these cell lines, we examined oxygen consumption as a direct measurement of mitochondrial respiration. Consistent with mitochondrial defects, A549-pBabe and A549-LKB1^{KD} cells had a lower basal rate of oxygen consumption rate (OCR) than the A549^{WT} cells (Figures 7D and S7C). Treatment of these cells with either phenformin or rotenone resulted in inhibition of mitochondrial respiration as shown by an acute drop OCR in levels (Figures S7C and S7D). OCR levels tracked inversely with mitotracker red staining here, consistent with the idea that the accumulated mitochondria in the LKB1-deficient cells are respiration defective.

Mitochondrial Complex I inhibition has been reported to induce reactive oxygen species (ROS) similar to that seen with Complex III inhibition (Hirst et al., 2008; Kushnareva et al., 2002). Thus, we next examined the release of mitochondrial reactive oxygen species (mtROS) following the treatment with phenformin, metformin, or the complex III inhibitor antimycin A and found that phenformin was a more potent inducer of mtROS than metformin (Figure S7E). Staining of A549-pBabe and A549-LKB1^{KD} cells showed modest elevations in mtROS compared to A549-LKB1^{WT} cells, both basally and following phenformin treatment (Figure 7E). To examine whether the doses of phenformin used in our therapeutic study were effective enough to induce LKB1-dependent effects on mitophagy, we performed western blot analysis of lung tumor nodules from mice with and without phenformin treatment for 5 days and discovered reduced phosphorylation of ULK1 and an accumulation of the mitophagy regulator Parkin in KL_{luc} but not K_{luc}, or KP_{luc} lung tumors (Figure 7F). These results suggest defects of the AMPK-ULK1 signaling

(D) Box plots representing the mean tumor burden following 3 weeks of treatment. Tumor burden was calculated by averaging the red pseudocolored tumor area from H&E-stained whole lung sections shown in (C) bottom panel.

(E) Representative images of H&E-, Ki67-, or TUNEL-stained K_{luc}, KL_{luc}, and KP_{luc} lung tumor sections. Ki67 or TUNEL positively stained cells (in green) and nuclei (in blue). Scale bar = 100 μm.

(F and G) Box plots representing the mean Ki67 (F) and TUNEL scores (G) from K_{luc}, KL_{luc}, and KP_{luc} mice treated with vehicle or phenformin. (*) Statistical significance ($p < 0.05$) calculated using a nonparametric one-way ANOVA (Tukey test).

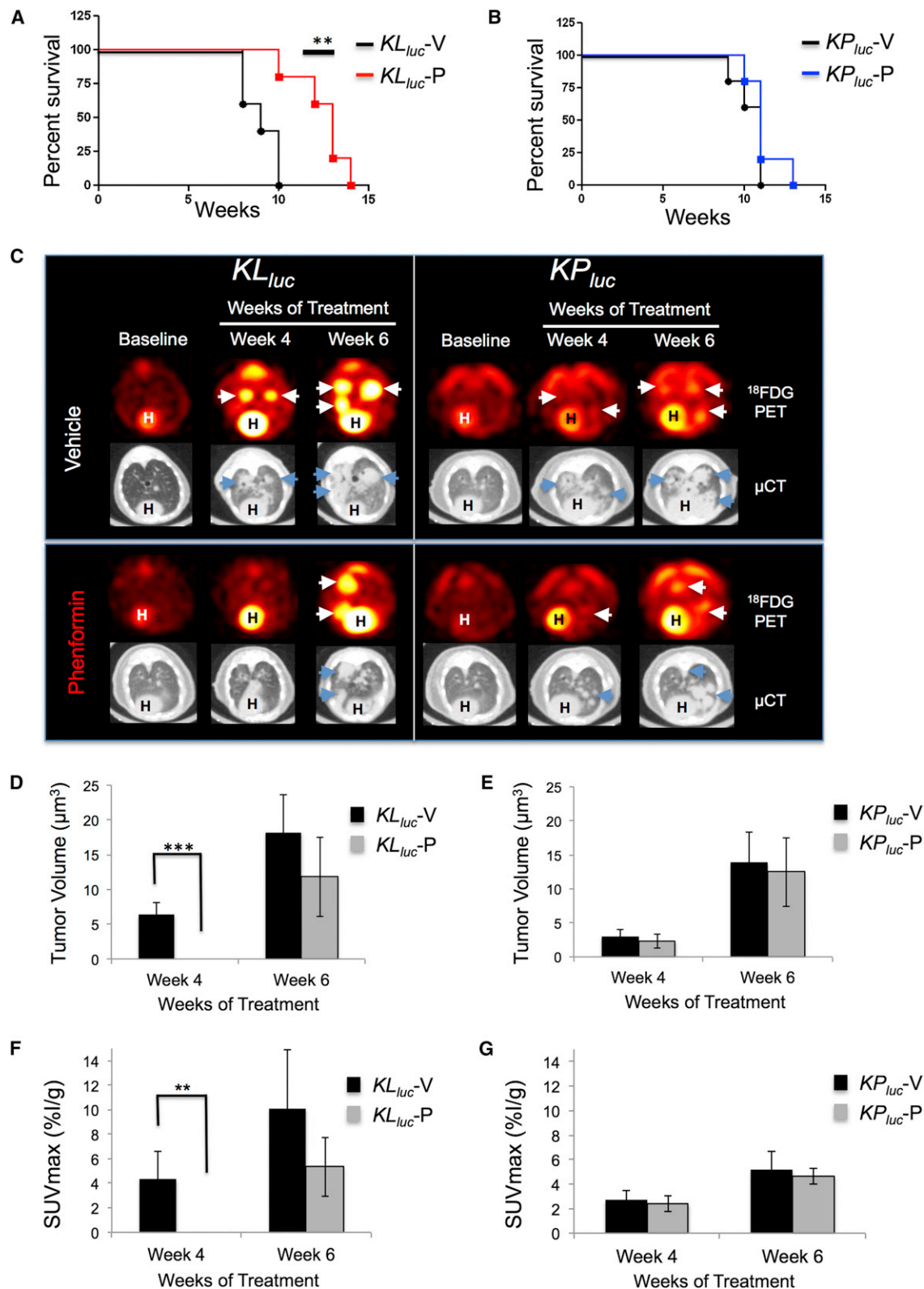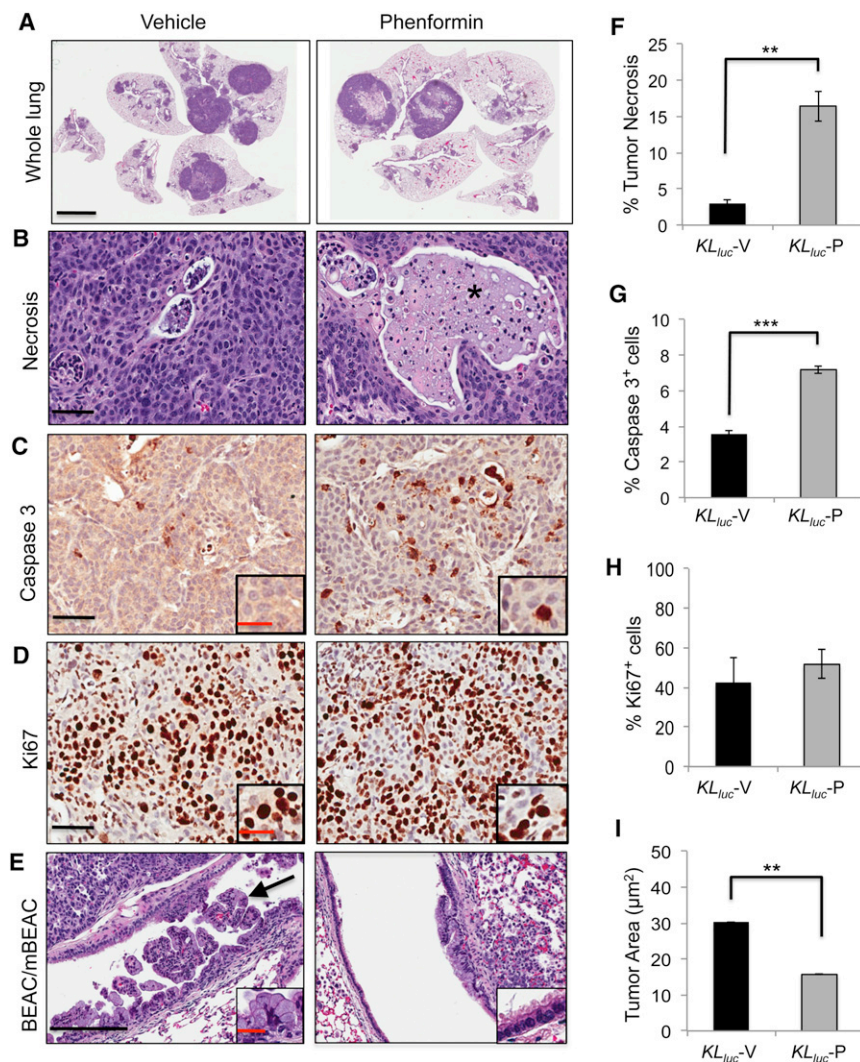All data are represented as the mean ± SEM. See also Figure S4.

Figure 5. Phenformin Significantly Increased Overall Survival and Slowed Tumor Progression in KL_{luc} Mice Shown by ^{18}FDG-PET and μCT Imaging

(A and B) Kaplan-Meier survival curves for KL_{luc} mice (A) or KP_{luc} mice (B) treated with vehicle (n = 5) or phenformin (n = 5) for each tumor genotype, respectively, with a **p = 0.008 for KL_{luc} mice determined by Wilcoxon logrank test.

(legend continued on next page)

Figure 6. Phenformin Induces a Significant Therapeutic Response in KL_{luc} Lung Tumors

(A) Hematoxylin and eosin (H&E)-stained whole lung sections of KL_{luc} mice treated with vehicle (saline) or phenformin, scale bar = 4 mm.

(B–E) Representative images of lung tumors from KL_{luc} mice treated with vehicle (saline) or phenformin. (B) Tumor necrosis, scale bar = 50 μm. (C) Activated caspase 3, scale bar = 50 μm. Inset represents magnification of caspase-3-stained cells, scale bar = 25 μm. (D) Ki67 stain, scale bar = 50 μm. Inset represents magnification of Ki67-stained cells, scale bar = 25 μm. (E) Mixture of bronchiolar-epithelial adenocarcinoma (BEAC) and mucinous bronchiolar-epithelial adenocarcinoma (mBEAC) shown with arrow, scale bar = 200 μm. Inset represents magnification of mBEAC cells, scale bar = 50 μm.

(F) Mean percentage of necrotic tumor area in vehicle- and phenformin-treated KL_{luc} mice. **p = 0.002.

(G) Mean percentage of tumor cell apoptosis from vehicle- and phenformin-treated KL_{luc} mice. ***p < 0.0001.

(H) Ki67 index for vehicle- and phenformin-treated KL_{luc} mice.

(I) Total BEAC and mBEAC tumor area (μm²) in vehicle- and-phenformin treated KL_{luc} mice. **p < 0.006. n = 5 KL_{luc} mice per treatment group (vehicle or phenformin). Statistical analysis performed using an unpaired Student's t test.

All data are represented as the mean ± SEM. See also Figure S6.

hyperactivation of mTORC1 in addition to other progrowth pathways (Shackelford and Shaw, 2009), initial interest has been in rapamycin analogs or other mTOR inhibitors. However, rapamycin treatment of an autochthonous lung tumor model with *Kras* and *Lkb1* mutations similar to the one used here showed a minimal therapeutic effect (Liang et al., 2010), perhaps because of the multitude of pathways deregulated from LKB1 deficiency that can still fuel tumorigenesis even when mTORC1 is suppressed. Hyperactivation of Src family kinases was also discovered as a biochemical marker and potential therapeutic target in *Lkb1*-deficient lung tumors (Carretero et al., 2010). Combination of the Src inhibitor dasatinib with PI3K and MEK inhibitors in similar mouse lung tumor models showed a synergistic tumor response, though dasatinib as a single agent displayed a minimal effect (Carretero et al., 2010). The fact that phenformin induces therapeutic response as a single agent taken together with the success of dasatinib

pathway and mitophagy in vivo following loss of LKB1 (Figure 7G), which may help sensitize these tumors to the effects of phenformin on mitochondrial integrity.

DISCUSSION

In this study we have found that the diabetes drug phenformin shows selective and significant antitumor activity in genetically engineered mouse models of lung cancer bearing LKB1 mutations. Molecular targeted therapeutics hold great promise for the future of cancer treatment, but for the 15%–30% of NSCLC bearing inactivating mutations in *LKB1*, there has been little in the way of targeted agents to date. As loss of LKB1 results in
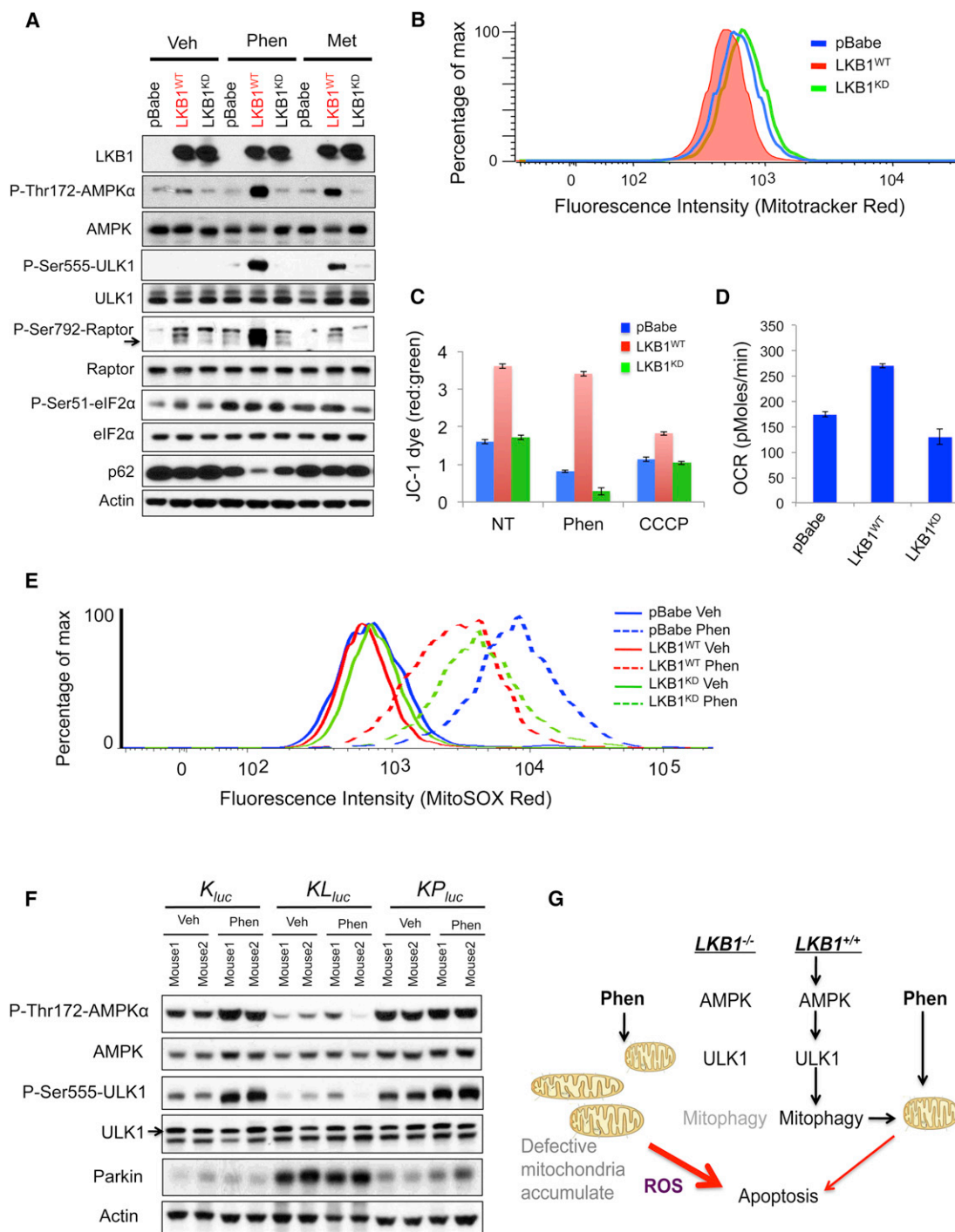
Figure 7. Mitochondrial Defects in LKB1$^{-/-}$ NSCLC Confer Sensitivity to Phenformin

(A) Lysates from A549-pBabe, A549-LKB1^{WT}, and A549-LKB1^{KD} cells were treated with vehicle (DMEM), phenformin (2 mM), or metformin (20 mM) for 4 hr and immunoblotted with the indicated antibodies.

(B) FACS analysis of cells from (A) stained with Mitotracker Red.

(C) Cells from (A) stained with JC-1 dye following 4 hr of treatment with vehicle (DMEM), phenformin (2 mM), metformin (20 mM), or CCCP (100 μM). Mitochondrial membrane potential (Δψ, red/green ratios) were measured by emission of red and green fluorescence using FACS.

(D) Oxygen consumption rate (OCR) of cells from (A).

(E) Cells from (A) were stained with MitoSOX Red following 16 hr of treatment with vehicle (DMEM) or phenformin (2 mM) and analyzed by FACS.

(F) Lung tumor lysates from K_{luc}, KL_{luc}, and KP_{luc} mice treated 5 days with vehicle or phenformin ad lib feeding were immunoblotted with the indicated antibodies.

(G) Model illustrating mitochondrial defects and phenformin induced cell death in $LKB1^{-/-}$-deficient tumor cells.

All data are represented as the mean ± SEM. See also Figure S7.

in combinations suggests that phenformin may also show greater success in defined combinations, which will be a focus for future investigations. Of relevance, a recent study treating the same three NSCLC models used here with a combination of standard-of-care docetaxel with MEK inhibitors revealed that *Kras; Lkb1* mutant tumors were selectively resistant to that combination, unlike *Kras* alone or *Kras; p53* mutant tumors (Chen et al., 2012). It is in the context of this body of work that selective sensitivity of *Kras; Lkb1* tumors to phenformin as a single agent in aggressive autochthonous models of lung cancer is so notable.

We have been interested in whether one could utilize metabolic stress-inducing compounds as anticancer agents for LKB1 mutant tumors in their autochthonous setting in the intact organism ever since we observed that LKB1-deficient cells were sensitive to apoptosis induced by metabolic stress in culture (Shaw et al., 2004). We focused our attention on the biguanide family of antidiabetes therapeutics for their ability to reduce intracellular ATP levels as a result of mitochondrial complex I inhibition. The absence of LKB1 signaling to AMPK means such cells will go for an extended time without activation of this sensor to restore ATP levels. We expect that mitochondrial damage and ATP loss also activate AMPK-independent stress sensing pathways, as we demonstrate here with multiple markers of the eIF2α signaling pathway. These findings are consistent with previous reports of AMPK-independent effects of biguanides (Foretz et al., 2010; Kalender et al., 2010). Our results are also consistent with recent studies demonstrating that AMPK mediates cell survival following metabolic stress not only through effects on ATP restoration but also by restoring NADPH levels, which are needed to neutralize ROS that arise during these stresses (Jeon et al., 2012). Inhibition of mitochondria complex I has been shown to cause ROS induction (Hirst et al., 2008; Kushnareva et al., 2002), so the fact that phenformin is a potent complex I inhibitor may underlie its ROS generation, which LKB1-deficient cells are genetically incapable of neutralizing efficiently. Future studies will be needed to fully assess the contribution of ROS in the LKB1-sensitive apoptosis following phenformin.

The biguanide metformin is the most widely used type 2 diabetes therapeutic worldwide and more recently has become used in treating other insulin-resistant conditions, including polycystic ovary syndrome (PCOS) (Motta, 2008). Metformin garnered considerable attention as a potential anticancer agent once the connection between LKB1 and AMPK was discovered (Birsoy et al., 2012; Taubes, 2012). As AMPK activation can be growth suppressive, diabetics taking these agents daily for decades might have a lowered incidence of cancer because of chronic effects from AMPK-mediated suppression of mTORC1 and other progrowth pathways, depending on how effective and sustained the clinical doses of metformin are at activating AMPK in different tissues. In addition, a non-cell-autonomous mechanism for metformin's antitumor effects may be its ability to lower circulating blood glucose and insulin levels, which also contribute to cancer risk and incidence in some contexts (Pollak, 2010). A number of epidemiological studies have found that diabetics taking metformin exhibit lowered risk of overall cancer compared to those taking other forms of diabetes medication (Dowling et al., 2012; Pollak, 2012). Given these observations, over 50 different clinical trials investigating the use of

metformin in oncology are currently underway (http://www.clinicaltrials.gov). Whether phenformin would yield similar broad anticancer results, given that it also effectively lowers blood glucose and also more potently activates AMPK across a wide-variety of tissues, remains to be investigated. As phenformin has a 50-fold greater potency than metformin for mitochondrial complex I inhibition (Owen et al., 2000; Dykens et al., 2008), part of its therapeutic success in cancer models when compared to metformin may be due to the fact that at maximal tolerated doses in rodents and clinically utilized doses in humans, one achieves greater ATP loss and ROS induction with phenformin. However, another distinction between these two biguanides is a greater tissue bioavailability for phenformin, which may be due to the apparent reliance of metformin on a tissue-restricted cell-surface transporter, Oct1, to efficiently cross the plasma membrane, unlike the more lipophilic phenformin (Hawley et al., 2010). Phenformin was removed from clinical use for type 2 diabetes because of incidence of fatalities from lactic acidosis (Crofford, 1995; Owen et al., 2000), reported in 64 cases per 100,000 patients per year, with patients bearing compromised kidney function at greatest risk. However, phenformin or another biguanide analog may still find utility as anticancer agents as the dosing and shorter duration in cancer therapy would be quite different from its prior clinical use for diabetes. Patients could also be prescreened for kidney function and other biomarkers to reduce any risk of lactic acidosis. Based on our findings here and previous studies of metformin, it seems most likely that phenformin might have potential use for early-stage lung tumors or as an adjuvant therapy following resection of early-stage NSCLC tumors. Although phenformin is unlikely to be suitable as a single-agent therapy in advanced-stage disease, it may synergize with other modalities, which warrants future investigation. A critical need for future clinical studies will be developing biomarkers of metformin and phenformin action in human tissues using clinically achievable doses (Pollak, 2010). Our identification of phospho-Ser51 eIF2α and its targets CHOP and BiP/Grp78 as AMPK-independent markers of phenformin-induced stress may prove valuable for such studies.

Whether *LKB1* deficiency confers sensitivity toward other agents that perturb ATP production via effects on mitochondria, glycolysis, or glutaminolysis also remains an interesting area for future targeted therapeutic development. Given the large percentage of sporadic lung, cervical, and endometrial cancers bearing *LKB1* mutations, identifying agents selectively targeting *LKB1* mutant tumors is a critical goal and one that seems particularly amenable to drugs targeting tumor metabolism.

EXPERIMENTAL PROCEDURES

Antibodies and Reagents

Antibodies from Cell Signaling Technologies (Danvers, MA, USA) used for immunoblots were diluted 1:1,000 and included LKB1 (D60C5) (#3047), phospho-AMPK Thr172 (#2531), total AMPK α1/2 (#2532), phospho-Raptor Ser792 (#2083), total Raptor (#2280), phospho-ULK1 (ser555) (#5869), eIF4E (#9742), phospho-eIF2α (ser51) (#3398), total eIF2α (#9722), cleaved caspase 3 (#9664), PARP (#9542), cleaved PARP (Asp214) (#5625), cleaved PARP mouse-specific (Asp214) (#9544), phospho-S6 (ser255/236) (#4858), S6 (#2217), phospho-4E-BP1 (thr37/46) (#2855), 4E-BP1 (#9644), phospho-IGF-IR/IR (#3024), IGF-IR/IR (#3027), phospho-AKT (ser473) (#4060), AKT

(#9272), CHOP (#5554), and BiP/GRP78 (#3177). Total ULK1 (A7481 WB 1:1,000) and anti-actin (A5441 WB1:5000) were purchased from Sigma-Aldrich (St. Louis, MO, USA). The p53 (CM5) antibody was obtained from Vector Labs (Burlingame, CA, USA; VP-P956 WB 1:1,000). The p62 antibody was obtained from Progen (Heidelberg, Germany; #GP62-C). AICAR was obtained from Toronto Research Chemicals (North York, Ontario, Canada). Phenformin, Metformin, and 2-deoxyglucose (2DG) and Antimycin A (cat. no. A8674); were purchased from Sigma-Aldrich. CCCP was obtained from the Molecular Probes JC-1 dye kit (Carlsbad, CA, USA; cat no. M34152).

Cell Culture

Cells were incubated at 37°C and maintained at 5% CO2. A549, H460, A427, H838, and HeLa cell lines were obtained from ATCC, and H157 cells were a kind gift from Dr. John Minna. Cells were grown in Dulbecco's modified Eagle's medium (DMEM) or RPMI 1640 medium (GIBCO) plus 10% fetal bovine serum (Hyclone, Logan, UT, USA) and penicillin and streptomycin. Retroviral gene expression was performed as described previously (Gwinn et al., 2008). Briefly, for retroviral infection, the pBabe, pBabe-FLAG-LKB1, and pBabe-FLAG-LKB1-KD (Addgene #'s 1764, 8592, and 8593) constructs were transfected along with the ampho packaging plasmid into growing HEK293T cells. Viral supernatants were collected 48 hr after transfection, spun for 5 min at 3,000 rpm, and filtered, and target cells were infected in the presence of polybrene. Twenty-four hours later, cells were selected with puromycin. Cells were plated at a density of 1×10^5 per well in 6-well dishes and grown for 18 hr before treatment.

Mouse Therapeutic Trials

Lox-Stop-Lox Kras^{G12D} were obtained from Tyler Jacks at Massachusetts Institute of Technology (Jackson et al., 2005) and *p53$^{lox/lox}$* mice from the Mouse Models of Human Cancers Consortium (Jonkers et al., 2001). *Lkb1$^{lox/lox}$* mice are as previously reported (Shaw et al., 2005). *Rosa26-Lox-Stop-Lox-Luc* mice were obtained from Jackson Laboratories (Bar Harbor, ME, USA) courtesy of Bill Kaelin (Safran et al., 2003). Mice were inbred on an FVB background. Lung tumors were induced by intranasal inhalation of 5×10^6 plaque forming units adeno-Cre (purchased from University of Iowa adenoviral core) as previously described (Jackson et al., 2005). Mice that displayed with clinical signs of disease, such as labored breathing or severe weight loss, were euthanized and necropsied. The mean tumor latencies we observed were comparable to previous studies with the exception of *KP$_{luc}$* mice, which developed large, aggressive lung tumors with the same latency of *KL$_{luc}$* mice (Jackson et al., 2005; Ji et al., 2007). In the experiments in Figure 4, mice were administered with vehicle (water), metformin, or phenformin (Toronto Research Corporation, Ontario, Canada) ad lib through their drinking water, and their daily intake of fluids were monitored. Fresh metformin (1.8 mg/ml) or phenformin (1.8 mg/ml) was administered every other day. Long-term treatments consisted of 3 weeks treatment (schematic in Figure S4D), and acute treatments lasted 5 days. For the intraperitoneal injections in Figure 4A, mice were given one injection of saline (0.9%), metformin (300 mg/kg), or phenformin (150 mg/kg) and euthanized at 1, 4, and 8 hr post-injection, and lung tissue was isolated. In the therapeutic trials in Figures 5 and 6 (schematized in Figure S5A), mice were administered phenformin (100 mg/kg/day) by o.p. once daily 6 days/week beginning at 3 weeks postde-livery of adenovirus expressing Cre. All experimental procedures performed on mice were approved by the Salk Institute and University of California at Los Angeles Institutional Animal Care and Use Committees.

Statistical Analysis Methods

Means were compared and p values determined by parametric or nonpara-metric ANOVA, and statistical test details and significance at $p < 0.05$ are indicated in the text and figure legends. Survival curves were computed using the Kaplan-Meier method. All statistical calculations were carried out using GraphPad Prism 5 software (San Diego, CA) or SAS 9.3 (SAS, Cary, NC). For analysis of SUVmax and tumor volume from FDG-PET and μCT imaging, comparisons were made between vehicle (V) versus Phenformin (P) treatments at week 7 and week 9. Values that were below the level of detection, referred to as left-censored observations, were coded with "zero", although the actual value may be above zero but is usually lower than the lowest observed value.

REFERENCES

Algire, C., Amrein, L., Bazile, M., David, S., Zakikhani, M., and Pollak, M. (2011). Diet and tumor LKB1 expression interact to determine sensitivity to anti-neoplastic effects of metformin in vivo. Oncogene *30*, 1174–1182.

Anisimov, V.N., Berstein, L.M., Egormin, P.A., Piskunova, T.S., Popovich, I.G., Zabezhinski, M.A., Kovalenko, I.G., Poroshina, T.E., Semenchenko, A.V., Provinciali, M., et al. (2005). Effect of metformin on life span and on the devel-opment of spontaneous mammary tumors in HER-2/neu transgenic mice. Exp. Gerontol *40*, 685–693.

Appleyard, M.V., Murray, K.E., Coates, P.J., Wullschleger, S., Bray, S.E., Kernohan, N.M., Fleming, S., Alessi, D.R., and Thompson, A.M. (2012). Phenformin as prophylaxis and therapy in breast cancer xenografts. Br. J. Cancer *106*, 1117–1122.

Birsoy, K., Sabatini, D.M., and Possemato, R. (2012). Untuning the tumor metabolic machine: Targeting cancer metabolism: a bedside lesson. Nat. Med. *18*, 1022–1023.

Buzzai, M., Jones, R.G., Amaravadi, R.K., Lum, J.J., DeBerardinis, R.J., Zhao, F., Viollet, B., and Thompson, C.B. (2007). Systemic treatment with the antidi-abetic drug metformin selectively impairs p53-deficient tumor cell growth. Cancer Res. *67*, 6745–6752.

Carretero, J., Shimamura, T., Rikova, K., Jackson, A.L., Wilkerson, M.D., Borgman, C.L., Buttarazzi, M.S., Sanofsky, B.A., McNamara, K.L., Brandstetter, K.A., et al. (2010). Integrative genomic and proteomic analyses identify targets for Lkb1-deficient metastatic lung tumors. Cancer Cell *17*, 547–559.

Chae, Y.C., Caino, M.C., Lisanti, S., Ghosh, J.C., Dohi, T., Danial, N.N., Villanueva, J., Ferrero, S., Vaira, V., Santambrogio, L., et al. (2012). Control of tumor bioenergetics and survival stress signaling by mitochondrial HSP90s. Cancer Cell 22, 331–344.

Chen, Z., Cheng, K., Walton, Z., Wang, Y., Ebi, H., Shimamura, T., Liu, Y., Tupper, T., Ouyang, J., Li, J., et al. (2012). A murine lung cancer co-clinical trial identifies genetic modifiers of therapeutic response. Nature 483, 613–617.

Crofford, O.B. (1995). Metformin. N. Engl. J. Med. 333, 588–589.

Ding, L., Getz, G., Wheeler, D.A., Mardis, E.R., McLellan, M.D., Cibulskis, K., Sougnez, C., Greulich, H., Muzny, D.M., Morgan, M.B., et al. (2008). Somatic mutations affect key pathways in lung adenocarcinoma. Nature 455, 1069–1075.

Dowling, R.J., Niraula, S., Stambolic, V., and Goodwin, P.J. (2012). Metformin in cancer: translational challenges. J. Mol. Endocrinol. 48, R31–R43.

Dykens, J.A., Jamieson, J., Marroquin, L., Nadanaciva, S., Billis, P.A., and Will, Y. (2008). Biguanide-induced mitochondrial dysfunction yields increased lactate production and cytotoxicity of aerobically-poised HepG2 cells and human hepatocytes in vitro. Toxicol. Appl. Pharmacol. 233, 203–210.

Egan, D.F., Shackelford, D.B., Mihaylova, M.M., Gelino, S., Kohnz, R.A., Mair, W., Vasquez, D.S., Joshi, A., Gwinn, D.M., Taylor, R., et al. (2011). Phosphorylation of ULK1 (hATG1) by AMP-activated protein kinase connects energy sensing to mitophagy. Science 331, 456–461.

El-Mir, M.Y., Nogueira, V., Fontaine, E., Avéret, N., Rigoulet, M., and Leverve, X. (2000). Dimethylbiguanide inhibits cell respiration via an indirect effect targeted on the respiratory chain complex I. J. Biol. Chem. 275, 223–228.

Evans, J.M., Donnelly, L.A., Emslie-Smith, A.M., Alessi, D.R., and Morris, A.D. (2005). Metformin and reduced risk of cancer in diabetic patients. BMJ 330, 1304–1305.

Farago, A.F., Snyder, E.L., and Jacks, T. (2012). SnapShot: Lung cancer models. Cell 149, 246, 246 e241.

Foretz, M., Hebrard, S., Leclerc, J., Zarrinpashneh, E., Soty, M., Mithieux, G., Sakamoto, K., Andreelli, F., and Viollet, B. (2010). Metformin inhibits hepatic gluconeogenesis in mice independently of the LKB1/AMPK pathway via a decrease in hepatic energy state. J. Clin. Invest 120, 2355–2369.

Gill, R.K., Yang, S.H., Meerzaman, D., Mechanic, L.E., Bowman, E.D., Jeon, H.S., Roy Chowdhuri, S., Shakoori, A., Dracheva, T., Hong, K.M., et al. (2011). Frequent homozygous deletion of the LKB1/STK11 gene in non-small cell lung cancer. Oncogene 30, 3784–3791.

Gwinn, D.M., Shackelford, D.B., Egan, D.F., Mihaylova, M.M., Mery, A., Vasquez, D.S., Turk, B.E., and Shaw, R.J. (2008). AMPK phosphorylation of raptor mediates a metabolic checkpoint. Mol. Cell 30, 214–226.

Hardie, D.G., Ross, F.A., and Hawley, S.A. (2012). AMPK: a nutrient and energy sensor that maintains energy homeostasis. Nat. Rev. Mol. Cell Biol. 13, 251–262.

Hawley, S.A., Ross, F.A., Chevtzoff, C., Green, K.A., Evans, A., Fogarty, S., Towler, M.C., Brown, L.J., Ogunbayo, O.A., Evans, A.M., and Hardie, D.G. (2010). Use of cells expressing gamma subunit variants to identify diverse mechanisms of AMPK activation. Cell Metab. 11, 554–565.

Hemminki, A., Markie, D., Tomlinson, I., Avizienyte, E., Roth, S., Loukola, A., Bignell, G., Warren, W., Aminoff, M., Höglund, P., et al. (1998). A serine/threonine kinase gene defective in Peutz-Jeghers syndrome. Nature 391, 184–187.

Hirst, J., King, M.S., and Pryde, K.R. (2008). The production of reactive oxygen species by complex I. Biochem. Soc. Trans. 36, 976–980.

Huang, X., Wullschleger, S., Shpiro, N., McGuire, V.A., Sakamoto, K., Woods, Y.L., McBurnie, W., Fleming, S., and Alessi, D.R. (2008). Important role of the LKB1-AMPK pathway in suppressing tumorigenesis in PTEN-deficient mice. Biochem. J. 412, 211–221.

Inoki, K., Zhu, T., and Guan, K.L. (2003). TSC2 mediates cellular energy response to control cell growth and survival. Cell 115, 577–590.

Jackson, E.L., Olive, K.P., Tuveson, D.A., Bronson, R., Crowley, D., Brown, M., and Jacks, T. (2005). The differential effects of mutant p53 alleles on advanced murine lung cancer. Cancer Res. 65, 10280–10288.

Jeon, S.M., Chandel, N.S., and Hay, N. (2012). AMPK regulates NADPH homeostasis to promote tumour cell survival during energy stress. Nature 485, 661–665.

Ji, H., Ramsey, M.R., Hayes, D.N., Fan, C., McNamara, K., Kozlowski, P., Torrice, C., Wu, M.C., Shimamura, T., Perera, S.A., et al. (2007). LKB1 modulates lung cancer differentiation and metastasis. Nature 448, 807–810.

Jin, S., DiPaola, R.S., Mathew, R., and White, E. (2007). Metabolic catastrophe as a means to cancer cell death. J. Cell Sci. 120, 379–383.

Jonkers, J., Meuwissen, R., van der Gulden, H., Peterse, H., van der Valk, M., and Berns, A. (2001). Synergistic tumor suppressor activity of BRCA2 and p53 in a conditional mouse model for breast cancer. Nat. Genet. 29, 418–425.

Kalender, A., Selvaraj, A., Kim, S.Y., Gulati, P., Brule, S., Viollet, B., Kemp, B.E., Bardeesy, N., Dennis, P., Schlager, J.J., et al. (2010). Metformin, independent of AMPK, inhibits mTORC1 in a rag GTPase-dependent manner. Cell Metab 11, 390–401.

Kushnareva, Y., Murphy, A.N., and Andreyev, A. (2002). Complex I-mediated reactive oxygen species generation: modulation by cytochrome c and NAD(P)+ oxidation reduction state. Biochem. J. 368, 545–553.

Laderoute, K.R., Amin, K., Calaoagan, J.M., Knapp, M., Le, T., Orduna, J., Foretz, M., and Viollet, B. (2006). 5′-AMP-activated protein kinase (AMPK) is induced by low-oxygen and glucose deprivation conditions found in solid-tumor microenvironments. Mol. Cell. Biol. 26, 5336–5347.

Liang, M.C., Ma, J., Chen, L., Kozlowski, P., Qin, W., Li, D., Goto, J., Shimamura, T., Hayes, D.N., Meyerson, M., et al. (2010). TSC1 loss synergizes with KRAS activation in lung cancer development in the mouse and confers rapamycin sensitivity. Oncogene 29, 1588–1597.

Memmott, R.M., Mercado, J.R., Maier, C.R., Kawabata, S., Fox, S.D., and Dennis, P.A. (2010). Metformin prevents tobacco carcinogen—induced lung tumorigenesis. Cancer Prev. Res. (Phila.) 3, 1066–1076.

Motta, D.A. (2008). Metformin in the treatment of polycystic ovary syndrome. Curr. Pharm. Des. 14, 2121–2125.

Muaddi, H., Majumder, M., Peidis, P., Papadakis, A.I., Holcik, M., Scheuner, D., Kaufman, R.J., Hatzoglou, M., and Koromilas, A.E. (2010). Phosphorylation of eIF2α at serine 51 is an important determinant of cell survival and adaptation to glucose deficiency. Mol. Biol. Cell 21, 3220–3231.

Nakada, D., Saunders, T.L., and Morrison, S.J. (2010). Lkb1 regulates cell cycle and energy metabolism in haematopoietic stem cells. Nature 468, 653–658.

Osoegawa, A., Kometani, T., Nosaki, K., Ondo, K., Hamatake, M., Hirai, F., Seto, T., Sugio, K., and Ichinose, Y. (2011). LKB1 mutations frequently detected in mucinous bronchioloalveolar carcinoma. Jpn. J. Clin. Oncol. 41, 1132–1137.

Owen, M.R., Doran, E., and Halestrap, A.P. (2000). Evidence that metformin exerts its anti-diabetic effects through inhibition of complex 1 of the mitochondrial respiratory chain. Biochem. J. 348, 607–614.

Pollak, M. (2010). Metformin and other biguanides in oncology: advancing the research agenda. Cancer Prev. Res. (Phila.) 3, 1060–1065.

Pollak, M.N. (2012). Investigating metformin for cancer prevention and treatment: the end of the beginning. Cancer Discov. 2, 778–790.

Safran, M., Kim, W.Y., Kung, A.L., Horner, J.W., DePinho, R.A., and Kaelin, W.G., Jr. (2003). Mouse reporter strain for noninvasive bioluminescent imaging of cells that have undergone Cre-mediated recombination. Mol. Imaging 2, 297–302.

Sakamoto, K., McCarthy, A., Smith, D., Green, K.A., Grahame Hardie, D., Ashworth, A., and Alessi, D.R. (2005). Deficiency of LKB1 in skeletal muscle prevents AMPK activation and glucose uptake during contraction. EMBO J. 24, 1810–1820.

Sanchez-Cespedes, M., Parrella, P., Esteller, M., Nomoto, S., Trink, B., Engles, J.M., Westra, W.H., Herman, J.G., and Sidransky, D. (2002). Inactivation of LKB1/STK11 is a common event in adenocarcinomas of the lung. Cancer Res. 62, 3659–3662.

Shackelford, D.B., and Shaw, R.J. (2009). The LKB1-AMPK pathway: metabolism and growth control in tumour suppression. Nat. Rev. Cancer 9, 563–575.

Shackelford, D.B., Vasquez, D.S., Corbeil, J., Wu, S., Leblanc, M., Wu, C.L., Vera, D.R., and Shaw, R.J. (2009). mTOR and HIF-1alpha-mediated tumor

metabolism in an LKB1 mouse model of Peutz-Jeghers syndrome. Proc. Natl. Acad. Sci. USA *106*, 11137–11142.

Shaw, R.J., Kosmatka, M., Bardeesy, N., Hurley, R.L., Witters, L.A., DePinho, R.A., and Cantley, L.C. (2004). The tumor suppressor LKB1 kinase directly activates AMP-activated kinase and regulates apoptosis in response to energy stress. Proc. Natl. Acad. Sci. USA *101*, 3329–3335.

Shaw, R.J., Lamia, K.A., Vasquez, D., Koo, S.H., Bardeesy, N., Depinho, R.A., Montminy, M., and Cantley, L.C. (2005). The kinase LKB1 mediates glucose homeostasis in liver and therapeutic effects of metformin. Science *310*, 1642–1646.

Shu, Y., Sheardown, S.A., Brown, C., Owen, R.P., Zhang, S., Castro, R.A., Ianculescu, A.G., Yue, L., Lo, J.C., Burchard, E.G., et al. (2007). Effect of genetic variation in the organic cation transporter 1 (OCT1) on metformin action. J. Clin. Invest. *117*, 1422–1431.

Taubes, G. (2012). Cancer research. Cancer prevention with a diabetes pill? Science *335*, 29.

Ye, J., Kumanova, M., Hart, L.S., Sloane, K., Zhang, H., De Panis, D.N., Bobrovnikova-Marjon, E., Diehl, J.A., Ron, D., and Koumenis, C. (2010). The GCN2-ATF4 pathway is critical for tumour cell survival and proliferation in response to nutrient deprivation. EMBO J. *29*, 2082–2096.